Supporting Information

Water Adsorption-Induced Color Sensor: Insight into the Sensing Mechanism and Interfacial Engineering for Improved Responsiveness

Tai Kobayashi, Ryosuke Nishikubo, Yusuke Tomiyori, Fumitaka Ishiwari, Daisuke Asakura, Eiji Hosono, Miho Kitamura, Hisao Kiuchi,* Yoshihisa Harada,* Akinori Saeki **

Mr. T. Kobayashi, Dr. R. Nishikubo, Prof. Dr. F. Ishiwari, Prof. Dr. A. Saeki
Department of Applied Chemistry, Graduate School of Engineering, The university of Osaka, 2-1 Yamadaoka, Suita, Osaka 565-0871, Japan
E-mail: nishikubo@chem.eng.osaka-u.ac.jp (R.N.), saeki@chem.eng.osaka-u.ac.jp (A.S.)

Dr. R. Nishikubo, Prof. Dr. F. Ishiwari, Prof. Dr. A. Saeki
Innovative Catalysis Science Division, Institute for Open and Transdisciplinary Research Initiatives (ICS-OTRI), The University of Osaka, 1-1 Yamadaoka, Suita, Osaka 565-0871, Japan.

Prof. Dr. F. Ishiwari
Faculty & Graduate School of Urban Environmental Science, Tokyo Metropolitan University, 1-1 Minami-Osawa, Hachioji-shi, Tokyo 192-0397, Japan.

Dr. Y. Tomiyori, Dr. H. Kiuchi, Prof. Dr. Y. Harada

Institute for Solid State Physics (ISSP), The University of Tokyo, Kashiwa, Chiba 277-8581, Japan.

E-mail: harada@issp.u-tokyo.ac.jp (Y.H.)

Dr. Y. Tomiyori

AGC Inc., Yokohama, Kanagawa, 230-0045, Japan.

Dr. H. Kiuchi

Research Center for Energy and Environmental Materials (GREEN), National Institute for Materials Science (NIMS), Tsukuba, Ibaraki 305-0044, Japan.

KIUCHI.Hisao@nims.go.jp (H.K.)

Dr. D. Asakura, Dr. E. Hosono

Research Institute for Energy Efficient Technologies, National Institute of Advanced Industrial Science and Technology (AIST), Tsukuba, Ibaraki 305-8585, Japan.

Dr. M. Kitamura

NanoTerasu Center, National Institutes for Quantum Science and Technology (QST), Sendai, Miyagi 980-8579, Japan

Table S1. Summary of the performance of color-recognizable single cell photodetectors. Our work shows a fast photovoltage-based response and recovery without external bias or impedance analysis. (ref. 4 is not self-powdered photodtector, and requires an impedance analyzer to obtain wavelength-dependent signals)

Photoactive material	Color recognition mechanism	Sensing color region	Response time	Recovery time	Ref.
TiO_2/ASIS	WDPE [a)]	UV to green	2–5 s	10 s	1
TiO_2/ASIS	RWDPE [b)]	UV to green	10–20 s	7 s	2
Perovskite	Difference of light penetration depth	Blue to red	0.57–3.92 s [c)]	10 s	3
Perovskite	Ion and charge migration	Blue to red	21.3 ms [d)]	- [e)]	4
Graphdiyne/ WSe_2	Charge carrier trapping	Blue to red	1 s	Few seconds (< 10 s)	5
Perovskite	Difference of light penetration depth	UV to green	-	-	6
TiO_2/ASIS	WDPE	UV to green	**150 ms**	**3.12 s**	**This work**

a) Wavelength-dependent photovoltaic effect (WDPE) is proposed to be related to the TiO_2 photocatalytic effect under UV irradiation.

b) Reversed-WDPE is proposed to be related to carrier trapping under visible light and detrapping by UV.

c) Response time is dependent on irradiation wavelength (400 nm: 1.75 s, 500 nm: 0.57 s, 650 nm: 3.92 s).

d) An impedance analyzer is required to obtain wavelength-dependent signal.

e) Hyphen (-) means that there is no description of response/recovery time in the paper.

Note S1. The thickness of the adsorbed H_2O on glass substrate/TiO_2 was estimated by analyzing the variation in the O *Ka* fluorescence intensity. The total O *Ka* intensity at 550 eV, which is non-resonant region, increased by 4.27% relative to the dry state in Figures S3c,d. This increase is attributed to the fact that the contribution of fluorescence generated from the water layer itself exceeds the attenuation of the signal from the underlying glass substrate/TiO_2 caused by the water overlayer. To quantify the water layer thickness (d_{H_2O}), we simply employed a three-layer model consisting of the water overlayer (Layer 2), the mp-TiO_2 film (Layer 1), and the glass substrate (Layer 0). The theoretical fluorescence intensity I_i from a layer i with thickness d_i can be expressed by integrating the X-ray production and attenuation over the depth z:

$$I_i = \int_0^{d_i} Q_i \cdot \exp(-\mu_i^* z) dz$$

where Q_i represents the effective oxygen fluorescence production factor proportional to the oxygen density and the absorption cross-section at the incident energy (550 eV). μ_i^* represents the effective linear attenuation coefficient considering the experimental geometry, defined as:

$$\mu_i^* = \rho_i \left(\frac{\mu_{i,\text{inc}}}{\sin\theta_{in}} + \frac{\mu_{i,\text{fluo}}}{\sin\theta_{out}} \right)$$

Here, ρ_i is the effective density of the layer. $\mu_{i,\text{inc}}$ and $\mu_{i,\text{fluo}}$ denote the mass attenuation coefficients for the incident (550 eV) and fluorescent (525 eV) X-rays, respectively. θ_{in} (90°) and θ_{out} (45°) are the incident and take-off angles. The integrated intensities for the water layer ((I_{H_2O}), the mp-TiO_2 layer (I_{TiO_2}), and the glass substrate ($I_{glass\ sub}$) are derived as:

$$I_{H_2O} = \int_0^{d_{H_2O}} Q_{H_2O} \cdot \exp\left(-\mu_{H_2O}^* z\right) dz$$

$$I_{TiO_2} = \exp\left(-\mu_{H_2O}^* \cdot d_{H_2O}\right) \cdot \int_0^{d_{TiO_2}} Q_{TiO_2} \cdot \exp\left(-\mu_{TiO_2}^* z\right) dz$$

$$I_{glass\ sub} = \exp\left(-\mu_{H_2O}^* \cdot d_{H_2O}\right) \cdot \exp\left(-\mu_{TiO_2}^* \cdot d_{TiO_2}\right) \cdot \int_0^{\infty} Q_{glass\ sub} \cdot \exp\left(-\mu_{glass\ sub}^* z\right) dz$$

Here, the parameters used for the calculation are listed in Tables S2 and S3. By fitting the total calculated intensity ($I_{total} = I_{H_2O} + I_{TiO_2} + I_{glass\ sub}$) to the experimental intensity ratio, the thickness of the water layer was calculated to be 10.0–12.4 nm.

Table S2. Density, thickness, and porosity of each layer used for the calculation.

	PCPDTBT (Layer 4)	SbSI:Sb_2S_3 (Layer 3)	H_2O (Layer 2)	mp-TiO_2 (Layer 1)	Glass substrate (Layer 0)
Density (g cm^{-3})	1.5 ± 0.1[7]	4.6 ± 0.2	1.0	4.26	2.6
Thickness (nm)	35 ± 10	40 ± 10	-	153 ± 30	∞
Porosity (%)	0	50 ± 10	0	57[a]	0

a) Porosity was experimentally obtained from the mass of mp-TiO_2 layer (0.10 ± 0.02 mg), thickness (153 ± 30 nm), and substrate size (4 × 0.9 cm^2).

Table S3. Mass attenuation coefficient of each element from the X-ray interaction database.[8]

Element	Mass attenuation coefficient (cm^2 g^{-1})	
	Incident X-ray at 550 eV	Fluorescent X-ray at 525 eV
H	49.18	57.29
C	10763	12106
N	15558	17327
O	20708	1199
Si	7851	8823
S	11688	13002
Ti	20011	22125
Sb	24024	3416
I	3679	3973

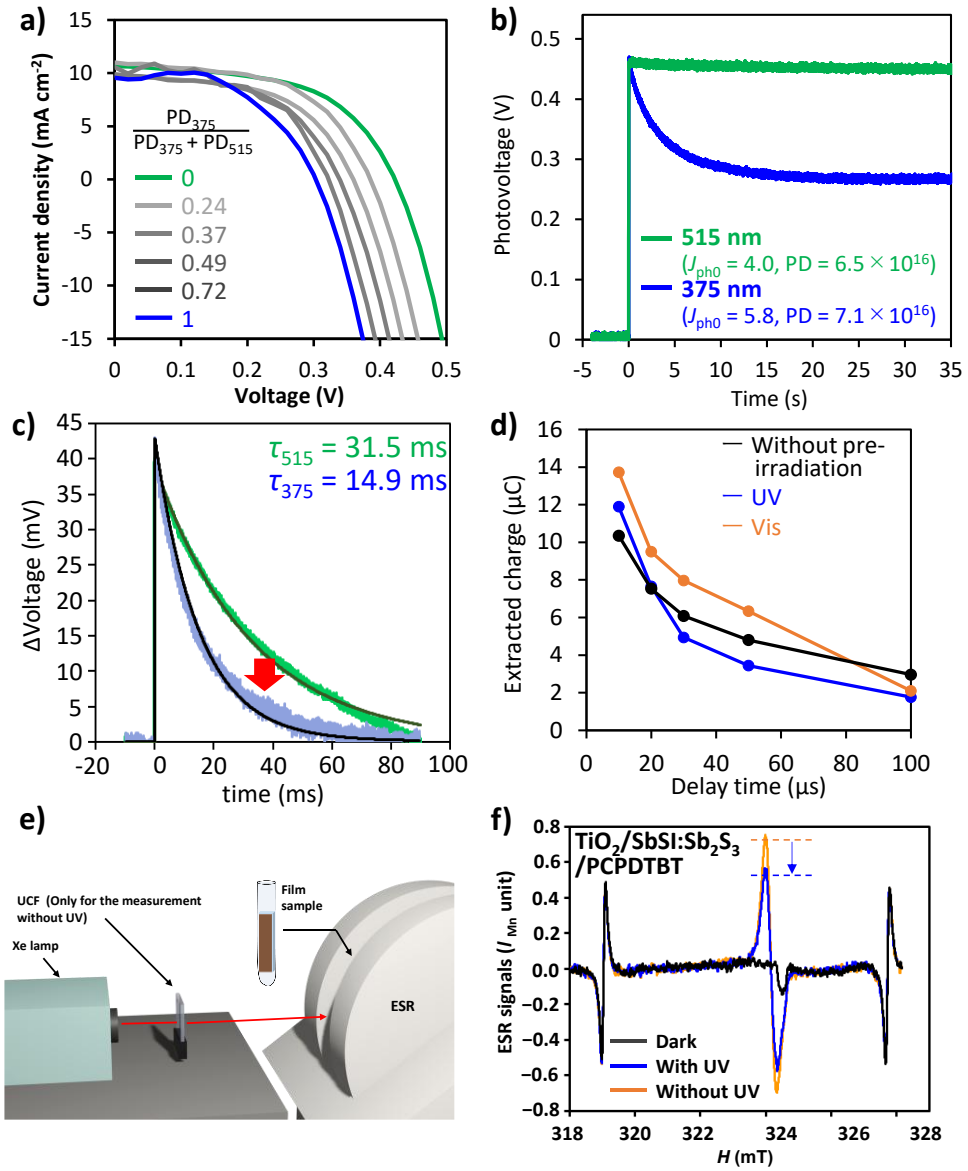

Figure S1. The wavelength dependent behavior of an SbSI:Sb_2S_3 photovoltaic (PV) device reported by our previous papers.[1,2] Wavelength-dependence of **a)** *JV* characteristics and **b)** time-dependent photovoltage (TDPV) decay. For TDPV measurement, the light intensity was modulated to output the close value of photocurrent. The corresponding short circuit photocurrent density (J_{ph0}, unit: mA cm^{-2}) and the irradiated photon density (PD, unit: photons cm^{-2} s^{-1}) are displayed in the graph. **c)** Transient photovoltage decay and **d)** extracted charge with different delay time obtained by charge extraction by linearly increasing voltage (CELIV) measurement. For this measurement, continuous UV or visible light was irradiated for 30 s, followed by a rapid integration (~5 s) under 532 nm pulse laser irradiation to obtain TPV or CELIV decay. **e)** The schematic image of operando electron spin resonance (ESR) measurement and **f)** the obtained ESR signals. Figures a-d and e-f are extracted from ref S1, S2, respectively.

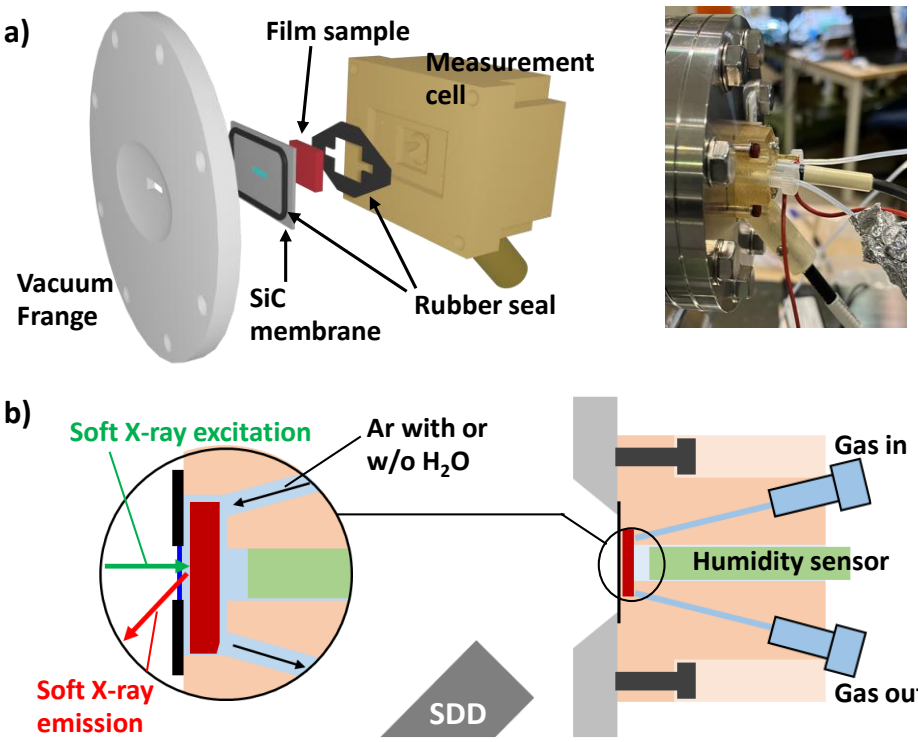

Figure S2. a) A schematic illustration of sample setting with the designed measurement cell and a picture of the measurement cell and connections. **b)** The schematic illustration of the detailed structure of the cell. "SDD" means silicon drift detector.

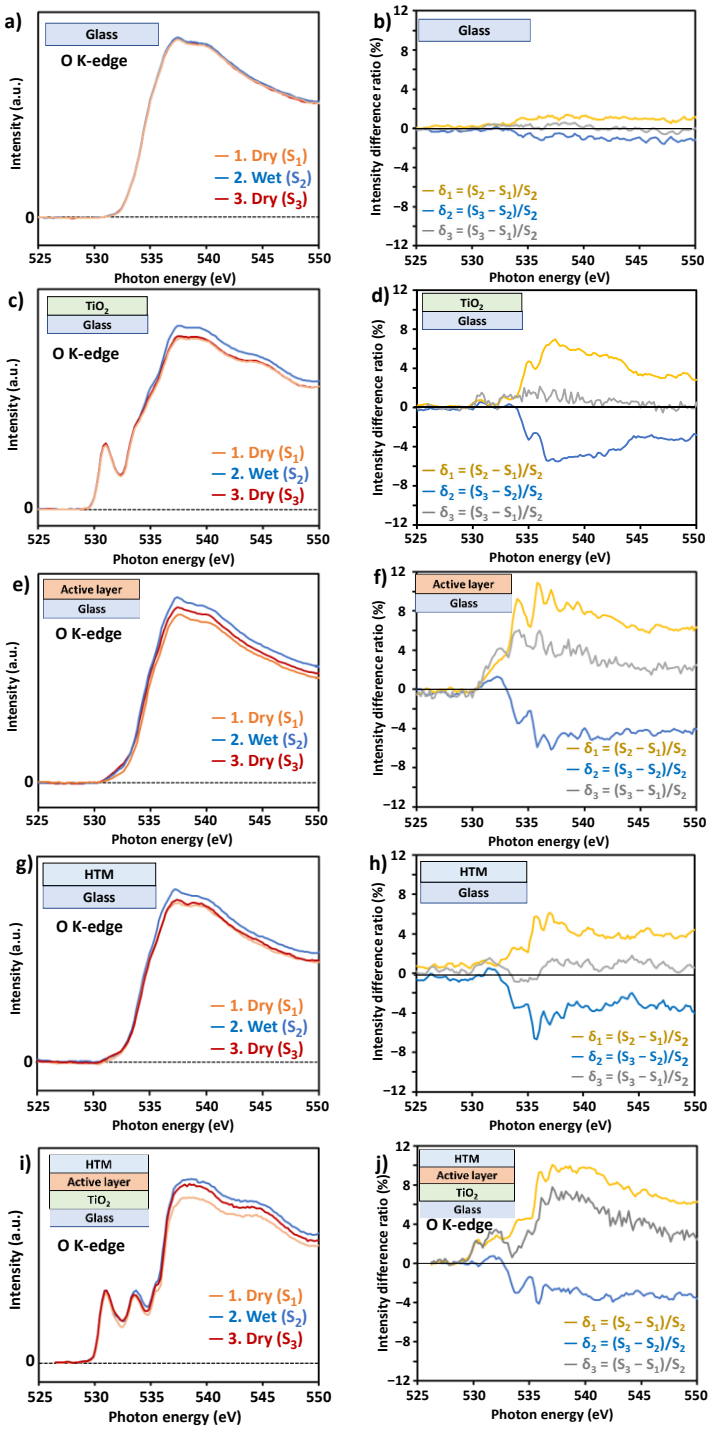

Figure S3. O K-edge XAS spectra and the corresponding difference spectra ratio of **a,b)** a glass substrate, **c,d)** TiO_2, **e,f)** ASIS, **g,h)** HTM, and **i,j)** TiO_2/ASIS/HTM. The difference spectra ratio (δ_1, δ_2 and δ_3) are calculated by $(S_2 - S_1)/S_2$, $(S_3 - S_2)/S_2$ and $(S_3 - S_1)/S_2$. Water adsorption onto bare glass was negligible (Figure S3a). It should be noted that normal glass substrates were used for **a-g**, while a quartz substrate was used for **i**. This is the reason for wider background spectra of **a-h** (533–550 eV) compared to that of **i** (536–550 eV).

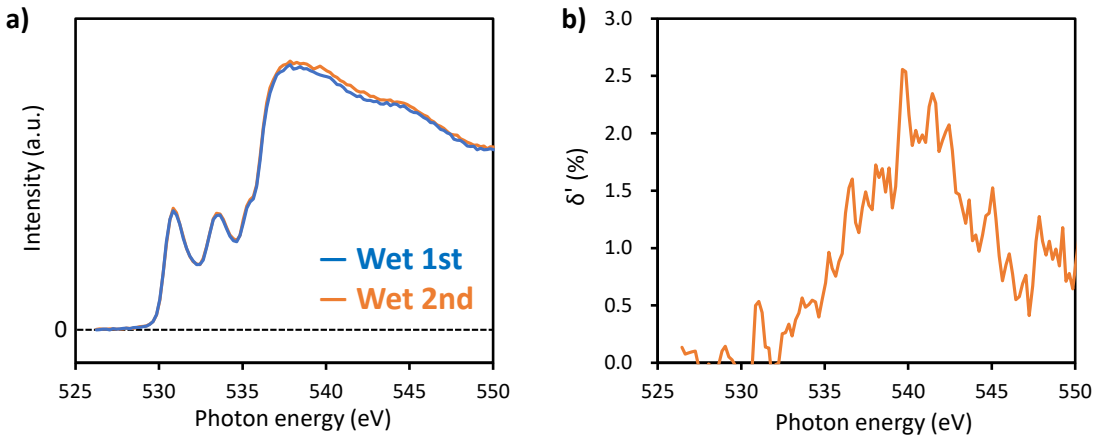

Figure S4. a) O K-edge XAS spectra of a tri-layer obtained by repeated measurement under high humidity, and **b)** the corresponding difference spectrum. The hydrophilization effect was observed when XAS measurements were repeated under high humidity.

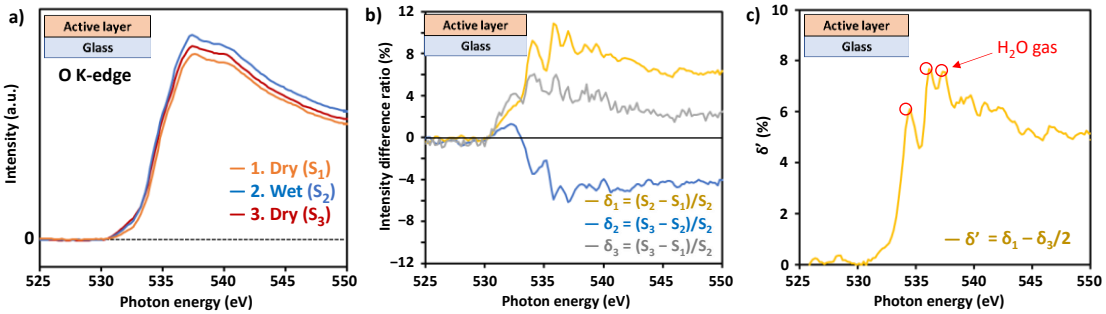

Figure S5. a) O K-edge XAS spectra of an ASIS single layer obtained under controlled humidity, **b)** the corresponding difference spectra ratio (δ_1, δ_2, δ_3), and **c)** the corrected difference spectra ratio (δ') are calculated by $\delta_1 - \delta_3/2$ (= $1 - (S_1 + S_3)/2S_2$). In δ' spectra, the hydrophilization effect is corrected by linear interpolation.

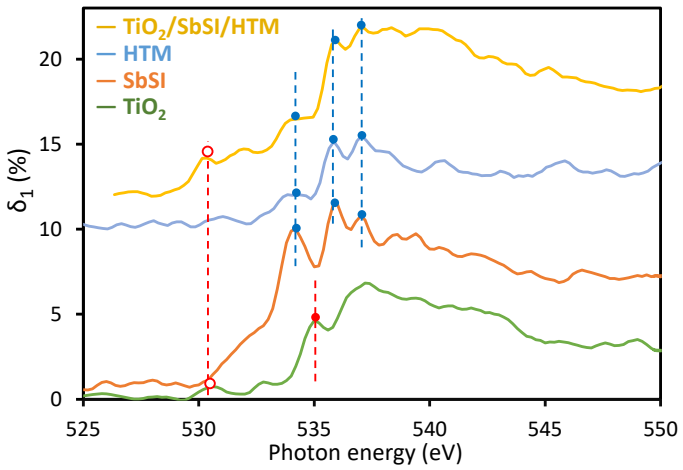

Figure S6. The difference XAS spectra ratio without correction (δ_1) of mono-layer films and a tri-layer film. The peaks attributed to gas and liquid-like H_2O are marked with blue and red dots, respectively. The pre-edge attributed to H_2O-TiO_2 interaction is marked with red circles. The spectra of SbSI, HTM, and a tri-layer are shifted along the vertical axis for easier comparison.

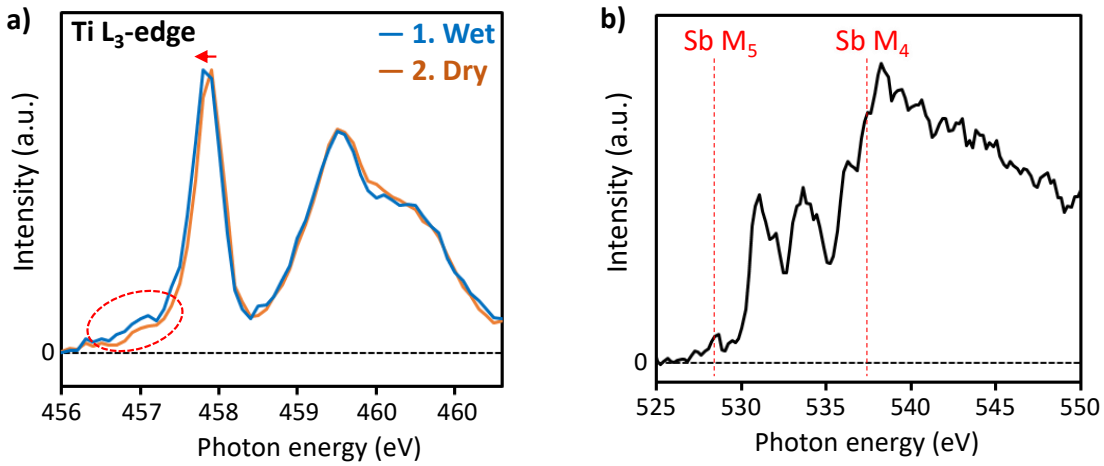

Figure S7. a) Ti L_3-edge XAS spectra of the TiO_2/ASIS/HTM tri-layer film obtained under controlled humidity. The spectra were normalized to the peak top intensity. **b)** Sb M-edge XAS spectra of the TiO_2/ASIS/HTM tri-layer film. The positions of the Sb M_5 and M_4 peaks were extracted from the data reported by Ye *et al*.[9]

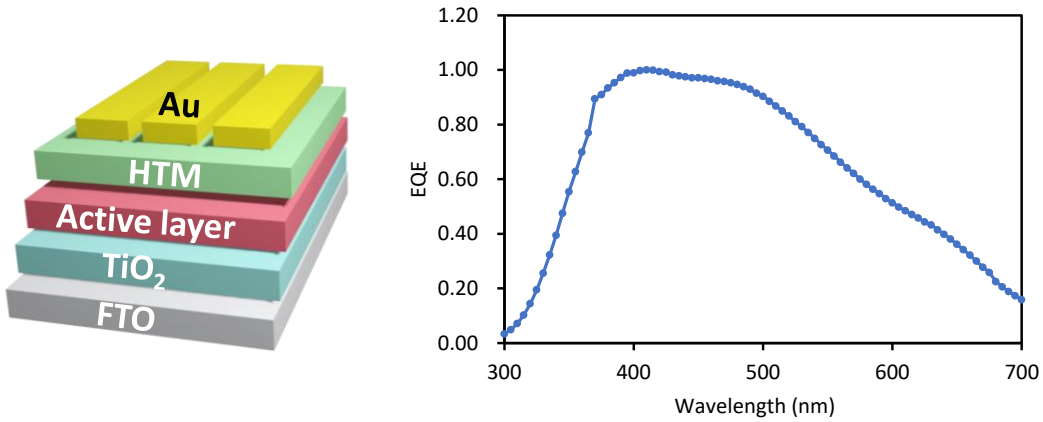

Figure S8. An illustration of the device structure used in this study and a normalized external quantum efficiency (EQE) spectrum corresponding to the spectra exhibited in Figure 3.

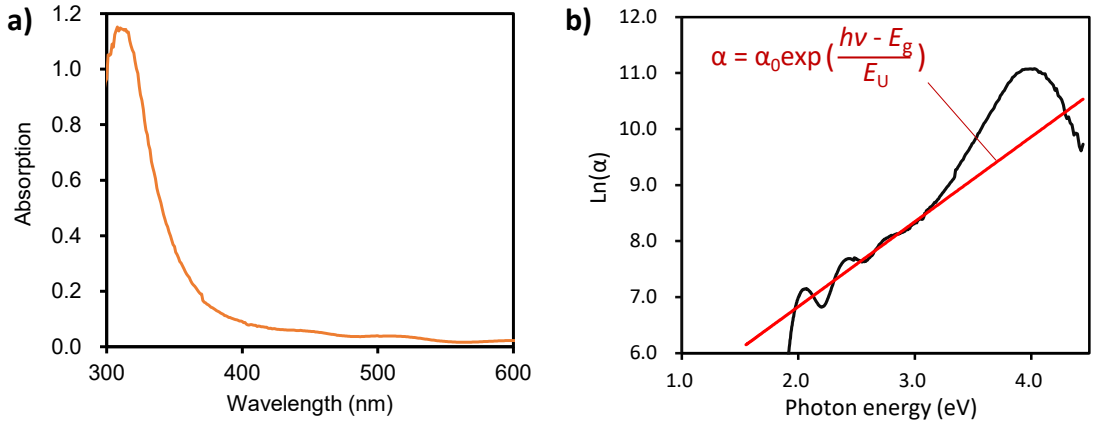

Figure S9. a) The photoabsorption spectrum and **b)** the corresponding Urbach tail analysis of a compact-TiO_2/mp-TiO_2 film. The Urbach energy (E_U) was calculated as 650–680 meV.

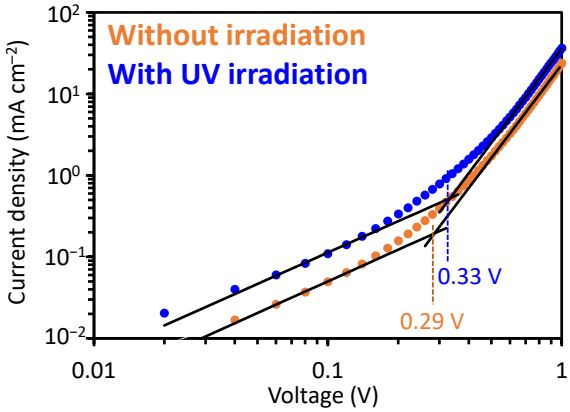

Figure S10 SCLC curve with and without UV irradiation. The device structure is FTO/TiO_2/ASIS/C_{60}/BCP/Au (electron only device). The measurement was performed before and after temporal UV irradiation (385 nm, 75 mW cm^{-2}, ~30 s). After UV irradiation was finished, *J-V* scan started immediately. The calculated trap density was 1.32×10^{17} and 1.53×10^{17} cm^{-3} for without and with UV irradiation, respectively. The measurements were performed with 0.02 V step, requiring approximately 9 s per scan. Hence, the actual trap density during UV irradiation should be higher than 1.53×10^{17} cm^{-3}.

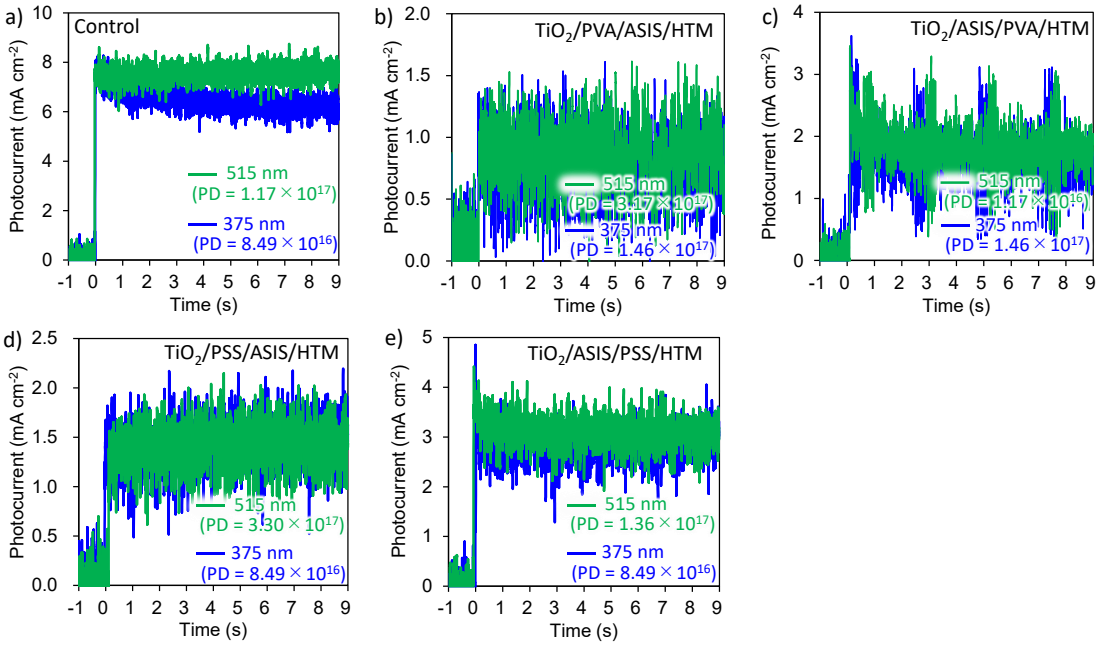

Figure S11. Time-dependent photocurrent (TDPC) decay of the devices **a)** without and **b-e)** with hydrophilic layer. The irradiated photon density (PD, unit: photons cm^{-2} s^{-1}) are displayed in the graph. The relatively low photo-current density of PVA- and PSS-included devices are due to insulating property of PVA and PSS.

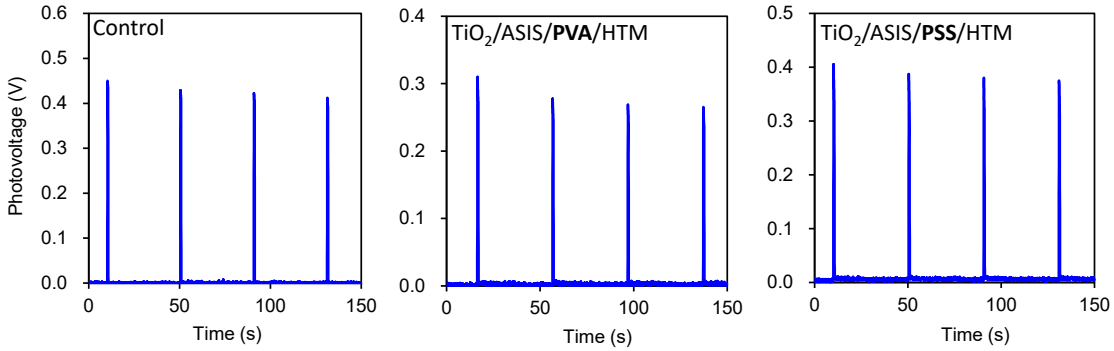

Figure S12. Periodic response of control, PVA- and PSS-incorporated devices upon 0.2s UV irradiation.

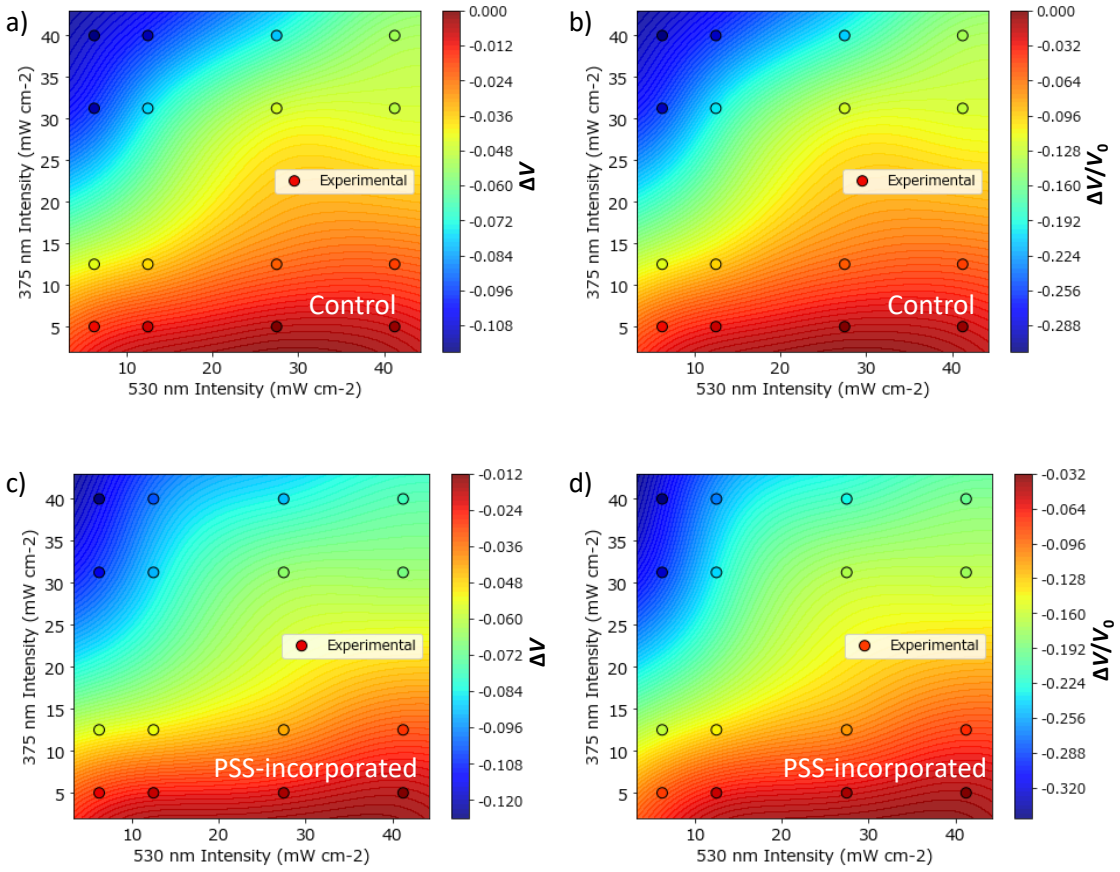

Figure S13. a, c) Photovoltage change (ΔV) and **b, d)** photovoltage change ratio ($\Delta V/V_0$) upon simultaneous irradiation of different color light with varied intensities. ΔV and V_0 are voltage decrease upon short 375 nm irradiation (0.5±0.1 s) and base photovoltage under constant 530 nm irradiation, respectively. The background color is a fitting by radial basis function (RBF) interpolation.

References

[1] R. Nishikubo, S. Li, A. Saeki, *Adv. Funct. Mater.* **2022**, *32*, 2201577/1–9.

[2] T. Kobayashi, R. Nishikubo, Y. Chen, K. Marumoto, A. Saeki, *Adv. Funct. Mater.* **2023**, *32*, 2311794/1–10.

[3] L. Min, Y. Zhou, H. Sun, L. Guo, M. Wang, F. Cao, W. Tian, L. Li, *Light Sci. & Appl.* **2024**, *13*, 280/1–11.

[4] Y. Zhou, H. Sun, L. Guo, S. Yang, L. Min, M. Wang, F. Cao, L. Li, *Adv. Mater.* **2025**, *37*, 2502889/1–9.

[5] H. Tang, W. Shi, W. Jiang, G. Wang, M. Tang, Z. Cai, R. Li, S. Wu, G. Zhang, J. Li, *Chem. Eng. J.* **2025**, *517*, 164215/1–9.

[6] C.-Y. Chang, Y.-L. Chin, C.-Y. Chang, J. Holovsky, *Adv. Funct. Mater.* **2025**, *35*, 2422732/1–15.

[7] C. S. Sarap, Y. Singh, J. M. Lane, N. Rai*, Sci. Rep.* **2023**, *13*, 21587.

[8] B. L. Henke, E. M. Gullikson, J. C. Davis, *Atomic Data and Nuclear Data Tables* **1993**, *54*, 181–342.

[9] M. Ye, T. Xu, G. Li, S. Qiao, Y. Takeda, Y. Saitoh, S.-Y. Zhu, M. Nurmamat, K. Sumida, Y. Ishida, S. Shin, A. Kimura, *Phys. Rev. B* **2019**, *99*, 144413.